REPORT DOCUMENTATION PAGE

Form Approved OMB NO. 0704-0188

1. REPORT DATE (DD-MM-YYYY)	2. REPORT TYPE	3. DATES COVERED (From - To)
08-10-2018	Final Report	9-Oct-2017 - 8-Jul-2018

4. TITLE AND SUBTITLE
Final Report: Plasma Processing of Sapphire Nanostructures for Low-Loss Multilayer Composites

5a. CONTRACT NUMBER
W911NF-17-1-0591

5b. GRANT NUMBER

5c. PROGRAM ELEMENT NUMBER
611102

6. AUTHORS

5d. PROJECT NUMBER

5e. TASK NUMBER

5f. WORK UNIT NUMBER

7. PERFORMING ORGANIZATION NAMES AND ADDRESSES
North Carolina State University
2701 Sullivan Drive
Admin Srvcs III, Box 7514
Raleigh, NC 27695 -7514

8. PERFORMING ORGANIZATION REPORT NUMBER

9. SPONSORING/MONITORING AGENCY NAME(S) AND ADDRESS (ES)
U.S. Army Research Office
P.O. Box 12211
Research Triangle Park, NC 27709-2211

10. SPONSOR/MONITOR'S ACRONYM(S)
ARO

11. SPONSOR/MONITOR'S REPORT NUMBER(S)
71897-MS-II.1

12. DISTRIBUTION AVAILIBILITY STATEMENT
Approved for public release; distribution is unlimited.

13. SUPPLEMENTARY NOTES
The views, opinions and/or findings contained in this report are those of the author(s) and should not contrued as an official Department of the Army position, policy or decision, unless so designated by other documentation.

14. ABSTRACT

15. SUBJECT TERMS

16. SECURITY CLASSIFICATION OF:			17. LIMITATION OF ABSTRACT	15. NUMBER OF PAGES	19a. NAME OF RESPONSIBLE PERSON
a. REPORT	b. ABSTRACT	c. THIS PAGE			Chih-Hao Chang
UU	UU	UU	UU		19b. TELEPHONE NUMBER 919-513-7968

RPPR Final Report
as of 09-Oct-2018

Agency Code:

Proposal Number: 71897MSII **Agreement Number: W911NF-17-1-0591**
INVESTIGATOR(S):

Name: Chih-Hao Chang
Email: cchang7@ncsu.edu
Phone Number: 9195137968
Principal: Y

Organization: **North Carolina State University**
Address: 2701 Sullivan Drive, Raleigh, NC 276957514
Country: USA
DUNS Number: 042092122 EIN: 566000756
Report Date: 08-Oct-2018 Date Received: 08-Oct-2018
Final Report for Period Beginning 09-Oct-2017 and Ending 08-Jul-2018
Title: Plasma Processing of Sapphire Nanostructures for Low-Loss Multilayer Composites
Begin Performance Period: 09-Oct-2017 **End Performance Period:** 08-Jul-2018
Report Term: 0-Other
Submitted By: Chih-Hao Chang Email: cchang7@ncsu.edu
Phone: (919) 513-7968
Distribution Statement: 1-Approved for public release; distribution is unlimited.

STEM Degrees: 0 **STEM Participants:** 2

Major Goals: Multilayer materials consisting of alternating ceramic and polymer layers are commonly found in naturally occurring nacre shell, and can find application as lightweight armor. However, such an architecture is generally opaque, and suffers from thin-film interference effects that lead to iridescence. Recent work by our group demonstrated that such optical limitations can be overcome by using interfacial nanostructures in silica-polymer multilayers, resulting in enhancement of optical transmission and suppression of iridescent effects [9,10]. However, challenges remain: (1) While the principle was demonstrated using silica, hard ceramics such as Al2O3 (sapphire) and AlON are more suitable for armor applications. These materials have higher refractive indices that can lead to higher optical losses. (2) Sapphire also has high mechanical hardness and is chemically stable, making it more resistant to micromachining. This can lead to challenges in controlling the profile of the interfacial nanostructures

The proposed research aims to investigate the plasma processing of sapphire and create surface nanostructures with well-defined geometry and order. Sapphire and other aluminum oxide materials have high optical transmission, mechanical hardness, strength, and toughness, and are attractive for armor material, nanophotonics, and solid-state lighting. However, they are also chemically inert and can be difficult to micromachining, especially for high density features. This research will examine the etching dynamics and physical/chemical reactions of nanostructured sapphire. We will develop novel lithographic and plasma etching processes to enable precise control of structure geometry and order. Furthermore, we will use the sapphire nanostructures as a basic building block to suppress reflection losses, iridescence, and scattering to enhance transmission of multilayer sapphire-polymer composites. This work can lead to lightweight transparent armor with enhanced toughness and broadband optical transmission, and contribute towards the Army's mission in blast/projectile mitigation.

Accomplishments: Please see attached PDF for final report and manuscript.

Training Opportunities: Nothing to Report

Results Dissemination: Nothing to Report

Honors and Awards: The PI Chih-Hao Chang was elevated to Senior Member by the Optical Society of America (OSA).

Protocol Activity Status:

RPPR Final Report
as of 09-Oct-2018

Technology Transfer: Nothing to Report

PARTICIPANTS:

Participant Type: PD/PI
Participant: Chih-Hao Chang
Person Months Worked: 1.00 **Funding Support:**
Project Contribution:
International Collaboration:
International Travel:
National Academy Member: N
Other Collaborators:

Participant Type: Graduate Student (research assistant)
Participant: Yi-An Chen
Person Months Worked: 9.00 **Funding Support:**
Project Contribution:
International Collaboration:
International Travel:
National Academy Member: N
Other Collaborators:

Participant Type: Graduate Student (research assistant)
Participant: Zhiren Luo
Person Months Worked: 3.00 **Funding Support:**
Project Contribution:
International Collaboration:
International Travel:
National Academy Member: N
Other Collaborators:

Plasma Processing of Sapphire Nanostructures for Low-Loss Multilayer Composites

(Final Report, grant #71897-MS-II)

Chih-Hao Chang

Associate Professor
Mechanical and Aerospace Engineering
North Carolina State University
Raleigh, NC 27695
Telephone: (919) 513-7968
Email: chichang@ncsu.edu

Submitted to:

Dr. Michael Bakas

Synthesis and Processing of Materials

Army Research Office

October 5, 2018

1. Statement of the Problem Studied

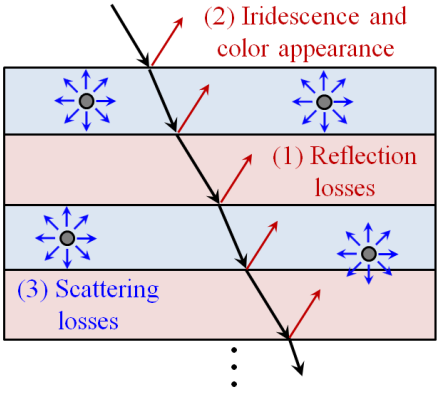

Figure 1. Optical losses due to reflection, interference, and scattering.

Multilayer materials consisting of alternating ceramic and polymer layers are commonly found in naturally occurring nacre shell, and can find application as lightweight armor [1-8]. However, such an architecture is generally opaque, and suffers from thin-film interference effects that lead to iridescence (**Figure 1**). Recent work by our group demonstrated that such optical limitations can be overcome by using interfacial nanostructures in silica-polymer multilayers, resulting in enhancement of optical transmission and suppression of iridescent effects [9,10]. However, challenges remain: **(1) While the principle was demonstrated using silica, hard ceramics such as Al_2O_3 (sapphire) and AlON are more suitable for armor applications**. These materials have higher refractive indices that can lead to higher optical losses. **(2) Sapphire also has high mechanical hardness and is chemically stable, making it more resistant to micromachining**. This can lead to challenges in controlling the profile of the interfacial nanostructures

The proposed research aims to investigate the plasma processing of sapphire and create surface nanostructures with well-defined geometry and order. Sapphire and other aluminum oxide materials have high optical transmission, mechanical hardness, strength, and toughness, and are attractive for armor material, nanophotonics, and solid-state lighting. However, they are also chemically inert and can be difficult to micromachining, especially for high density features. This research will examine the etching dynamics and physical/chemical reactions of nanostructured sapphire. We will develop novel lithographic and plasma etching processes to enable precise control of structure geometry and order. Furthermore, we will use the sapphire nanostructures as a basic building block to suppress reflection losses, iridescence, and scattering to enhance transmission of multilayer sapphire-polymer composites. This work can lead to lightweight transparent armor with enhanced toughness and broadband optical transmission, and contribute towards the Army's mission in blast/projectile mitigation.

2. Summary of the Most Important Results

In this project we successfully 1) investigated plasma etching of sapphire and fabricated the **highest density periodic sapphire nanostructures reported**, 2) **proposed a two-step etch mechanisms** for the plasma processing of sapphire, and 3) demonstrated **multilayer optical transmission enhancement** in silica-polymer composite over broad wavelength band and wide incident angle [16]. These results will be discussed in the following sections:

2.1) <u>Investigation of sapphire plasma etching.</u> It is widely understood that Cl-based gases such as BCl_3 and Cl_2 are effective RIE processes to etch Al. These gases react with Al to form etch product $AlCl_3$, which is a volatile species at low pressure. Br-based chemistry such as HBr is also effective, forming the volatile product $AlBr_3$. Previous work in the literature has demonstrated etching of Al_2O_3 films [11,12], sapphire substrates [13-15], and microstructures [16-18]. However the demonstrated structure are typically in micrometer scale and have high surface roughness. For our work we examined BCl_3, Cl_2, and HBr etch chemistry using inductively coupled plasma RIE system. The pure Cl_2 etch is used for Al etching, but has demonstrated low etch rates for Al_2O_3. The addition of BCl_3 improves the removal of alumina by

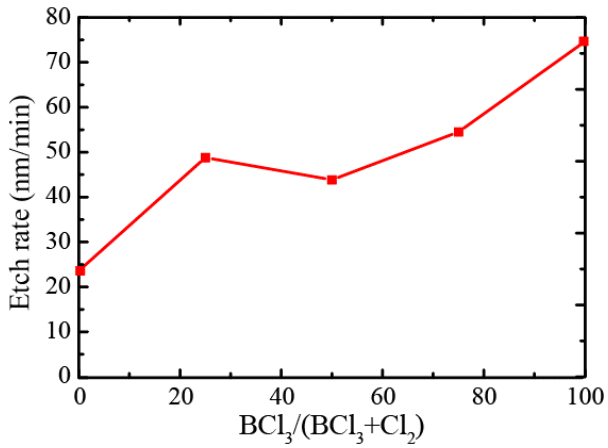

Figure 2. Sapphire etch rate vs relative BCl_3 flow rate, highlighting the role of Al_2O_3 reduction.

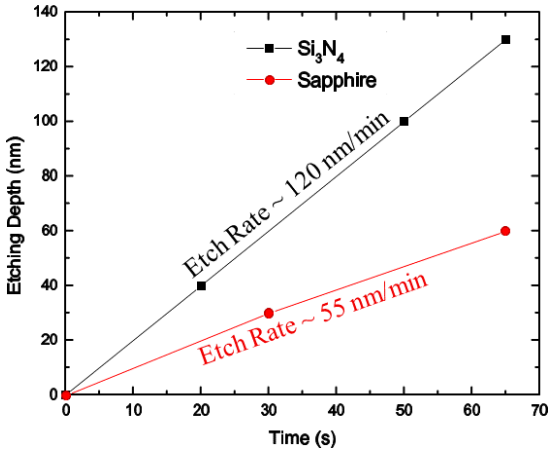

Figure 3. Etch depth of sapphire and Si_3N_4 (SiN) using 1:1 HBr/BCl_3 RIE.

reducing Al_2O_3 to Al, which can then react with Cl or Br ions to form a volatile species and be etched. The importance of the reducing agent can be seen in **Figure 2**, where the etch rate of a bulk sapphire substrate is plotted vs the relative flow rates of BCl_3/Cl_2. The etch conditions are total volume flow rate of 50 sccm, pressure of 10 mTorr, 500 W ICP power, and 200 V DC bias. It can be observed that the etch rate doubles when the BCl_3 flow rate is increased from 0% to 25%, indicating the critical role of Al_2O_3 reduction. Further increases in BCl_3 also results in higher etch rate after an initial decline. This results points to the importance of the reduction step.

The sapphire nanostructure etching experiments were conducted using single-crystal C-plane (0001) sapphire substrates, and a 120 nm-thick layer of SiN was deposited using plasma-enhanced chemical vapor deposition (PECVD) as the etch mask. Using interference lithography, periodic grating structures with 300 nm period were patterned into photoresist and then etched into SiN using CHF_3 RIE. A number of sapphire RIE chemistries were investigated, including Cl_2, BCl_3:HBr = 1:2, and BCl_3:HBr = 1:1. For Cl_2, this has resulted in a slow etch rate of 35 nm/min for nanopatterned sapphire, which is limited by physical sputtering of the solid alumina. The addition of BCl_3 with HBr improves the etch rate of sapphire nanostructures, increasing to 45 and 55 nm/min for BCl_3:HBr ratios of 1:2 and 1:1, respectively. Note the nanostructure etch rates agree with the unpatterned substrates results shown in **Figure 2**, where higher relative BCl_3 concentration improves etch rate. The measured etch depth vs time is plotted in **Figure 3** for sapphire and the mask material SiN. It can be seen that the etch selectivity is poor, which limits the structure aspect ratio and may lead to surface roughness.

The cross-section scanning electron microscope (SEM) images of the structure after sapphire etching is shown in **Figure 4**. Here a layer of SiN remains on the sapphire nanostructures, with little polymer residual on top. **Figure 5** depicts periodic structure with 120 nm width and 65 nm height was transferred into the sapphire substrate using 1:1 HBr/BCl_3 RIE. **These results are the highest density sapphire periodic features reported in the literature.** The structure is also smooth and has relatively low surface roughness when compared with other results. However, the aspect ratio of the structure is low, which can be attributed to the poor selectivity between sapphire and the etch mask. To increase aspect ratio, better understanding of the sapphire etch mechanism is needed to facilitate design of more effective etch process.

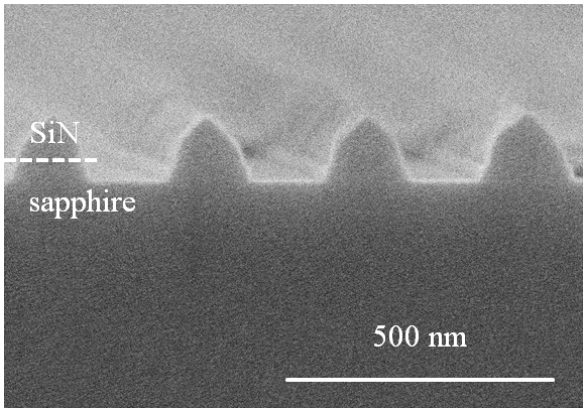

Figure 4. SEM of etched sapphire substrate with residual SiN film. A step between the sapphire/SiN interfaces can be observed.

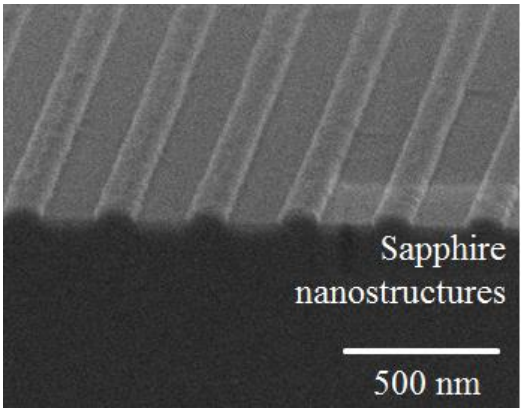

Figure 5. SEM of fabricated sapphire nanostructures with 120 nm features and 65 nm height using HBr/BCl_3 RIE.

2.2) Hypothesis of sapphire etch mechanism. One of the key goal of this work is to identify the key steps in sapphire etching. Our initial results point to a two-step mechanism, where Al_2O_3 is reduced to Al before effective etching using Cl or Br-based chemistry can take place. This is explained using a model etch system using BCl_3, as illustrated in **Figure 6**. First, BCl_3 is adsorb onto Al_2O_3 surface and dissociates. BCl_3 is a strong reduction agent, reducing Al_2O_3 to Al. The B atoms then react with O to form the by-products $B_xCl_yO_z$. The remaining Cl reacts with Al to form the volatile compound $AlCl_3$, completing the etching process. In the proposed two-step process, we believe the initial Al_2O_3 reduction process is critical and must be thermodynamically favorable and should form a volatile species. Additional Cl_2 can also be introduce to increase the Al etching rate if the reduction process is sufficient. Following this general model, the two-step mechanism is also applicable to other etch systems that consist of a reducing agent and a primary etch gases that form volatile species with Al.

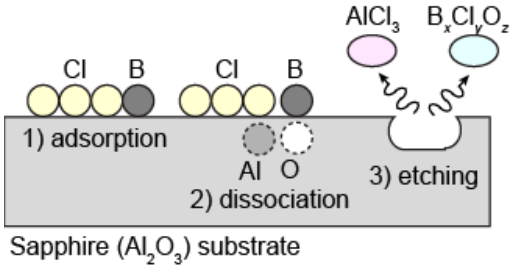

Figure 6. Proposed two-step sapphire etch mechanism. The process is initiated by the reduction of Al_2O_3 to Al, which forms $AlCl_3$. By-products $B_xCl_yO_z$ are generated.

To better understand the etch process, we examined *in situ* monitoring of the reaction gas species using a custom-built optical emission spectrometer (OES). This system can examine the optical emission within the plasma chamber to identify the gas species. This can be used to determine the by-product and etch product concentrations, and point to the particular chemical reactions taking place. In contrast to traditional post-process etch rate measurement, this real-time approach can shed light on the mechanisms as it occurs. Measured emission spectra using a prototype *in situ* OES is shown in **Figure 7**. Here the optical emission between 200-800 nm is measured for Cl_2 RIE of sapphire substrate. The emission wavelengths associated with Cl and Cl_2^+ radicals can be observed, as well as the primary etch product AlCl

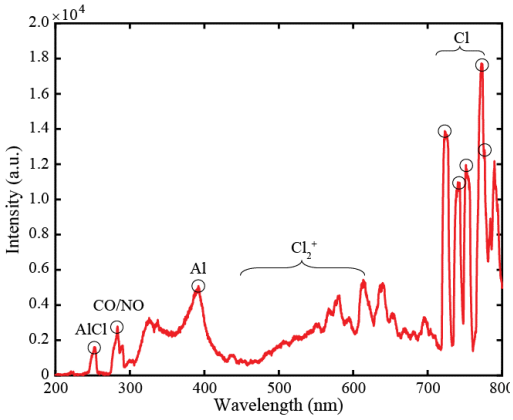

Figure 7. Measured OES signal for RIE of sapphire substrate using Cl_2.

at 260 nm. Another peak around 283-286 nm can be associated with CO or NO, which is attributed to residuals in the chamber. Note the AlCl peak is relatively weak and it is not possible to directly calculate the gas concentrations, two main drawbacks of OES. To validate the two-step reduction and etching mechanism, on-going work is examining the relative concentrations of the primary etch products and by-products in a BCl_3/Cl_2 system.

2.3) Scalability demonstration of enhanced optical transmission in multilayer composites. Another key accomplishment of this research is to demonstrate that light transmission can be enhanced in a multilayer composite systems by integrated nanostructures at the interface. In previous research we have shown that the transmission of a single nanostructured silica-polymer interface can be enhanced. In this research we demonstrated the scalability of the enhance transmission to multiple layers. We successfully fabricated 3 double-side patterned silica substrates, which were bonded by two epoxy layers to form a silica-polymer-silica-polymer-silica composite. The total thickness of the sample was around 2 mm. The measured transmission at 633 nm for the thick 3-layer silica-polymer composite with and without the interfacial nanostructures are shown in **Figure 8**. The experiment results show that under illumination TE polarized light, the transmission is enhanced by 7% at normal incidence, and up to 30% at 60-70º incident angle ranges. For the maximum incident angle of 70º, the measured transmission for the composite with and without the nanostructures are 72% and 46%, respectively. More layer integration can lead to even more enhancement, but the presence of particle defects in a university research environment makes demonstration difficult. However this work demonstrates that such scaling is possible and there are no known technical barriers.

The broadband transmittance of the 3-layer silica-polymer composite with and without the nanostructures at the interfaces was also characterized at normal incidence, as shown in **Figure 9**. The measurement data illustrates that up to 7% enhancement can be observed at 450 nm to 800 nm wavelength, with a peak transmission of 97% compared with 90% without the nanostructures. The enhancement is reduced at wavelength below 450 nm, and the transmission of the two samples are similar. This can be attributed to the relatively large structure period of 250 nm, which means diffracted orders in the UV can exist in the higher index polymer. The UV-curable epoxy also absorbs in the UV, therefore reducing transmission for both samples.

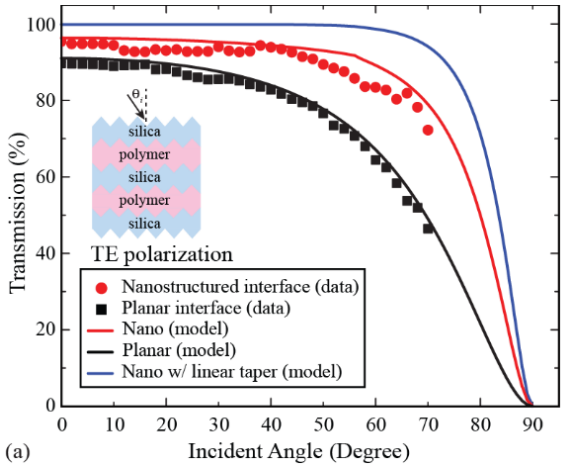

Figure 8. Transmission measurement and simulation vs incident angle for a thick 3-layer silica-polymer multilayer composite with and without interfacial nanostructures.

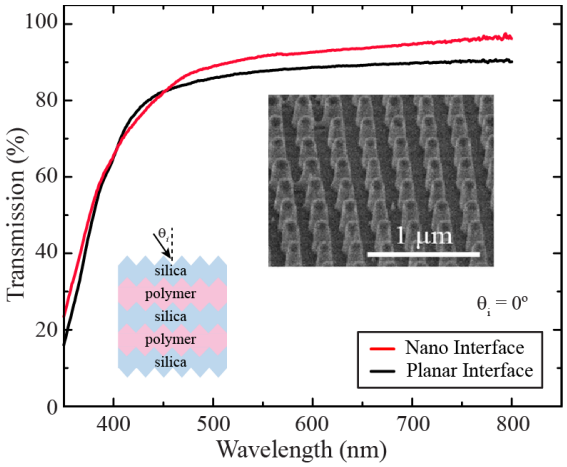

Figure 9. Broadband transmittance measurements of a 3-layer silica-polymer multilayer composite with and without interfacial nanostructures at 0º incident angle.

These results demonstrate that by using interfacial nanostructures, the reflection between two materials can be successfully suppressed. This effect in turn suppresses interference in multilayer composites, allowing for wavelength and angle-independent optical behavior.

3. Future Work

This research indicates that while it is possible to create high-density sapphire nanostructures, as demonstrated in our experimental results, increasing the structure aspect ratio is much more challenging. This is attributed to the low etch selectivity, which greatly limits the geometry that can be enable. To further advanced the processing of sapphire and enable nanopatterning, the etch mechanisms in plasma etching must be better understood. Based on our preliminary results, we propose a two-step mechanism, where the etching is initiated by the reduction of Al_2O_3 to Al, which can then form volatile gas species with Cl and Br-based chemistry. Our preliminary data including etch rates, OES signals, and analysis of etch profile support the proposed hypothesis, but more work is need to examine the reaction dynamics and balance between the Al_2O_3 reduction and Al etching process. A better understand of the etch mechanisms can lead to higher density, higher aspect ratio sapphire nanostructures that can be the building blocks for multifunctional materials, optoelectronic/photonic nanodevices, and high strength, high toughness transparent material.

Bibliography

1. A. P. Jackson, J. F. V. Vincent, and R. M. Turner, "The Mechanical Design of Nacre," *Proc. R. Soc. Lond. B*, vol. 234, no. 1277, pp. 415–440, 1988.
2. R. Z. Wang, Z. Suo, A. G. Evans, N. Yao, and I. A. Aksay, "Deformation mechanisms in nacre," *Journal of Materials Research*, vol. 16, no. 09, pp. 2485–2493, 2001.
3. F. Barthelat, C.-M. Li, C. Comi, and H. D. Espinosa, "Mechanical properties of nacre constituents and their impact on mechanical performance," *J. of Materials Research*, vol. 21, no. 08, pp. 1977–1986, 2006.
4. Z. Tang, N. A. Kotov, S. Magonov, and B. Ozturk, "Nanostructured artificial nacre," *Nature Materials*, vol. 2, no. 6, pp. 413–418, 2003.
5. X. Li, W.-C. Chang, Y. J. Chao, R. Wang, and M. Chang, "Nanoscale Structural and Mechanical Characterization of a Natural Nanocomposite Material: The Shell of Red Abalone," *Nano Lett.*, vol. 4, no. 4, pp. 613–617, 2004.
6. P. Podsiadlo, A. K. Kaushik, E. M. Arruda, A. M. Waas, B. S. Shim, J. Xu, H. Nandivada, B. G. Pumplin, J. Lahann, A. Ramamoorthy, and N. A. Kotov, "Ultrastrong and Stiff Layered Polymer Nanocomposites," *Science*, vol. 318, no. 5847, pp. 80, 2007.
7. E. Munch, M. E. Launey, D. H. Alsem, E. Saiz, A. P. Tomsia, and R. O. Ritchie, "Tough, Bio-Inspired Hybrid Materials," *Science*, vol. 322, no. 5907, pp. 1516, 2008.
8. J. Wang, Q. Cheng, and Z. Tang, "Layered nanocomposites inspired by the structure and mechanical properties of nacre," *Chem. Soc. Rev.*, vol. 41, 1111–1129, 2012.
9. Q. Yang, X. A. Zhang, A. Bagal, W. Guo, and **C.-H. Chang**, "Antireflection Effects at Nanostructured Material Interfaces and the Suppression of Thin-Film Interference," *Nanotechnology*, **24**, 235202 (2013).
10. Y.-A. Chen, S. V. Naidu, Z. Luo, and **C.-H. Chang**, "Design of Interfacial Antireflection Nanostructures in Multilayers," *61st International Conference on Electron, Ion, and Photon Beam Technology and Nanofabrication*, May 30, 2017, Orlando, FL. *Manuscript in review, October 2018*.
11. D.-P. Kim, J.-W. Yeo, and C.-I. Kim, "Etching properties of Al2O3 films in inductively coupled plasma," *Thin Solid Films*, vol. 459, no. 1–2, pp. 122–126, Jul. 2004.
12. S.-M. Koo, D.-P. Kim, K.-T. Kim, and C.-I. Kim, "The etching properties of Al2O3 thin films in N2/Cl2/BCl3 and Ar/Cl2/BCl3 gas chemistry," *Materials Science and Engineering: B*, vol. 118, no. 1–3, pp. 201–204, Apr. 2005.
13. Y. P. Hsu et al., "ICP etching of sapphire substrates," *Optical Materials*, vol. 27, no. 6, pp. 1171–1174, Mar. 2005.
14. Y. J. Sung et al., "High rate etching of sapphire wafer using Cl2/BCl3/Ar inductively coupled plasmas," *Materials Science and Engineering: B*, vol. 82, no. 1–3, pp. 50, 2001.
15. C. H. Jeong, D. W. Kim, H. Y. Lee, H. S. Kim, Y. J. Sung, and G. Y. Yeom, "Sapphire etching with BCl3/HBr/Ar plasma," *Surface and Coatings Technology*, vol. 171, no. 1, pp. 280–284, Jul. 2003.
16. C. H. Jeong et al., "Dry etching of sapphire substrate for device separation in chlorine-based inductively coupled plasmas," *Materials Science and Engineering: B*, vol. 93, no. 1–3, pp. 60–63, May 2002.
17. J. D. B. Bradley, F. Ay, K. Wörhoff, and M. Pollnau, "Fabrication of low-loss channel waveguides in Al2O3 and Y2O3 layers by inductively coupled plasma reactive ion etching," *Applied Physics B*, vol. 89, no. 2–3, pp. 311–318, Nov. 2007.
18. S.-H. Park, H. Jeon, Y.-J. Sung, and G.-Y. Yeom, "Refractive sapphire microlenses fabricated by chlorine-based inductively coupled plasma etching," *Appl. Opt., AO*, vol. 40, no. 22, pp. 3698–3702, Aug. 2001.

Enhancing optical transmission of multilayer composites using interfacial nanostructures

Yi-An Chen, Sharan V. Naidu, Zhiren Luo, and Chih-Hao Chang[*]

Department of Mechanical and Aerospace Engineering, North Carolina State University, Raleigh, North Carolina 27695, United States

*Corresponding author: *chichang@ncsu.edu*

ABSTRACT

We demonstrate the suppression of light reflections at solid-solid interfaces in multilayer thin and thick films using interfacial nanostructures. The embedded nanostructures have subwavelength features, and function as gradient-index medium to eliminate Fresnel losses induced by refractive index mismatch between dissimilar materials. Suppressing the interfacial reflection can reduce interference effects in thin films, and transmittance measurements of a polymer film on nanostructured silica substrate demonstrates a two-fold decrease in interference fringe contrast. A thick multilayer composite consisting of three fused silica and two polymer layers have also been fabricated and demonstrates enhancement of optical transmission up to 30%. The experimental results agree well with simulation models based on rigorous coupled-wave analysis, which predicts that further improvements can be achieved using optimized tapered profile. This work indicates that interfacial nanostructures can improve broadband and wide-angle response of multilayers, and can find applications in thin-film optoelectronic devices and composite windows.

KEYWORDS: Material interface, interfacial nanostructures, nanostructure fabrication, subwavelength structures, multilayers.

INTRODUCTION

In recent years, bioinspired nanostructures have drawn increasing interest because of their novel physical behaviors. One example is the antireflection (AR) nanostructures inspired by the moth eye, which can reduce light reflection on material surfaces [1–12]. The surface reflection can be attributed to refractive index mismatch at the air-solid interface, which causes Fresnel reflection losses [4,5,10] and reduces transmission. The moth-eye structures serve as a gradient-index medium where its effective index bridges the index mismatch [13]. Such an effect operates over broad wavelength band and wide viewing angle, which is advantageous over traditional AR coating [14,15]. Researchers have tried to solve the problem of reducing the reflected light and thereby increasing the transmission. Some methods have been demonstrated such as engineered surfaces can suppress surface reflections by using electron-beam [5,9], interference lithography [4,12,16], colloidal assembly [17,18], and maskless reactive ion etching [19] by researchers. A way to achieve a gradient-index AR medium [10,20,21] is to deposit oblique-angle of single layer and multilayers films with varying porosity. These advances have many applications in fabricating photonics and optoelectronics devices, such as optical micro-resonators [22] and light-emitting diodes [23]. Also these advances can enable anti-glare, self-cleaning windows [12], and improve the devices performance, such as improving efficiency of solar cells [24–27], enhancing light extraction in light emitting devices [28].

While most existing work on AR nanostructures has been focused on material surfaces, Fresnel losses can also occur between two solid materials. This is especially important in multilayer thin films, where multiple interfacial reflections must be

considered. Under coherent illumination, such reflections can interfere and induce iridescent effects. This can lead to wavelength and angle-dependent properties, which is undesirable in broadband optical element and devices. In our prior work, we have demonstrated that the interfacial reflection between a polymer film and silicon substrate can be suppressed using nanostructures by studying the reflectance spectra [29]. However, the optical behavior of the transmitted light into the substrate were not studied. The previous study also focused on a single interface, and the more complex phenomenon of reflections from multiple interfaces have not been examined. The question of how multiple interfacial reflections affect the broadband transmission in multilayer thin or thick films remain unanswered. These effects are illustrated in Fig. 1(a), where reflected orders at each interface can interfere. These losses may be mitigated by introducing tapered nanostructures at the interfaces, as illustrated in Fig. 1(b). The structures emulate as an effective medium with continuously changing index and bridges the neighboring refractive indices. These interfacial nanostructures can reduce the reflections at the interfaces, thereby suppressing iridescent effects induced by interference and increasing light transmission.

In this work, we report the experimental demonstration of interfacial nanostructures in multilayer thin and thick films to suppress interference effects and enhance broadband transmission. The structures are fabricated on fused silica substrates, serving as a template to create a nanostructured interface by infiltration using different polymer type and thickness. A substrate bonding process is used to stack and assemble multiple double-side patterned fused silica substrates, and a thick multilayer composite material consisting of three silica and two polymer layers have been successfully fabricated. The wide-angle and broadband optical performance of these structures were characterized and demonstrate

suppressed iridescence and enhanced transmission. The experimental data agree well with constructed simulation models based on rigorous coupled-wave analysis (RCWA) methods [30,31]. The results demonstrate that interfacial nanostructures are an effective method to mitigate wavelength and angle-dependent behavior and enhance broadband transmission in multilayers devices and composite materials.

FABRICATION METHOD AND MATERIALS

The proposed interfacial nanostructures is demonstrated in a composite multilayer with alternating polymer and fused silica layers. The structures are patterned using a combination of interference lithography (IL), reactive ion etching (RIE), and substrate stacking, as shown in Fig. 2. First, a fused silica substrate is spin coated with 13 nm antireflection coating (ARC i-con-7, Brewer Science) and 250 nm photoresist (PFI-88A2, Sumitomo), as shown in Fig. 2(a). The ARC film is used to reduce reflection from the substrate during lithography. Two-dimensional (2D) pillar array is then patterned in the photoresist using two orthogonal exposures in a Lloyd's mirror IL setup [12,32] as illustrated in Fig. 2(b). The structure has 250 nm period. The pattern is then transferred to the underlying fused silica substrate using O_2 and CHF_3 reactive ion etching (RIE). The photoresist mask is also etched during the process, yielding the tapered profile as illustrated in Fig. 2(c). After spin coating a protective polymer film (ProTEK B3-25, Brewer Science) on the front-side nanostructures, the same process is then repeated to pattern the backside of the fused silica substrate, as shown in Fig. 2(d). The ProTek film can be removed in a solvent solution (ProTEK Remover 100, Brewer Science) followed by O_2 plasma etching. This results in a fused silica substrate with subwavelength AR structures patterned on both sides. The double-side patterned fused silica substrates can then be bonded using a UV-

curable epoxy (NOA 170, Norland Optical Adhesive), as depicted in Fig. 2(e). The sample is cured in UV light with low intensity over an hour to reduce bubble formation. The thickness of the epoxy is typically in the order of 0.1 mm. This process can be repeated to construct a thick multilayer silica/polymer composite material with nanostructures embedded at each interface, as shown in Fig. 2(f). Three fused silica substrates, each 0.5 mm thick, have been bonded to yield a silica-polymer-silica-polymer-silica composite. Note each layer in the composite material is relatively thick compare to the coherent length of ambient light or broadband lamps, meaning that no interference is expected so that the transmission enhancement can be better quantified.

This fabrication process was also used to pattern a thin single-layer polymer sample to examine the effect of thin-film interference on the broadband transmittance. These samples consist of tapered nanostructures patterned on the front side of the fused silica substrate, as illustrated in Fig 2(c). A thin layer of photoresist (Sumitomo PFI-88) around 750 nm thick is then spin coated on top of fused silica nanostructures. The back side of the substrate is polished but not patterned. These samples therefore consist of a nanostructured polymer-silica interface, while the top polymer and bottom fused silica surfaces are planar. Here the film thickness is less than the coherent length of the spectrophotometer, allowing the study of interfacial reflection by quantifying the thin-film interference effects. Note these samples serve a different purpose to the thick multilayer samples described in the previous paragraph, which consists of tapered nanostructure on both sides for transmission characterization.

The scanning electron microscope (SEM) images of the fabricated nanostructures on the front fused silica substrate are shown in Figure 3. The top view of 2D pillar array in

photoresist after IL exposure is shown in Fig. 3(a), indicating periodic order in a square lattice. A few photoresist structure collapse can be seen. The side-view SEM of AR nanostructures etched into the fused silica substrate are shown in Fig. 3(b) and (c). The conic profile of the structure can be observed in the higher magnification image shown in Fig. 3(b). The large-area uniformity is illustrated in Fig. 3(c), with some defects due to residual connection between the structures. Some nanoscale spikes can also be observed, and can be attributed to redeposition of the volatile species during RIE. These results illustrate that the AR nanostructures are well arranged with 250 nm period and around 400 nm height, as desired. Few defects as a result of collapsed resist and surface roughness can be observed. The SEM images of the back-side structures indicate similar structure geometry and quality.

The optical properties of the thin and thick multilayer stacks with interfacial nanostructures are modeled using RCWA, where the tapered nanostructures are approximated by discrete 2D gratings with varying duty cycles. The RCWA model is based on alternating polymer (n = 1.70) and fused silica (n = 1.45) layers periodic along both x and y directions. The nanostructure model is approximated as a square lattice with a 250 nm period. Theoretical models for three types of structure at the interface have been constructed to validate experimental results and evaluate the effectiveness of the interfacial nanostructures. The first is a planar model consisting of continuous polymer film on fused silica substrate layers with no nanostructures. The second describes the fabricated samples with the nanostructured interface. The structure geometry and profile are obtained from the SEM images to accurately simulate the fabricated structure shape. The modeled structure has 400 nm height and 0 to 0.6 duty cycle. Note the fabricate structure height and profile

have not been optimized for AR performance, and taller structures with 700 to 800 nm height with more effective tapered profile can be achieved using different etching mask [10]. The third model consists of theoretical structures with 750 nm height and a linear tapered profile from 0 to 1 duty cycle, which describes the performance that can be obtained for more optimized structure geometry.

RESULTS AND DISCUSSION

The fused silica substrate with a thin photoresist film was characterized to study the thin-film interference effects. The broadband transmittance of the thin-film sample with planar and nanostructured interfaces were measured using a UV-visible-NIR spectrophotometer (Cary 5000, Agilent Co.), as shown in Figure 4. The transmittance measurements from 450 to 800 nm wavelength for incident angles $\theta_i = 0^o$ and 30^o are shown in Fig. 4(a) and (b), respectively. Intensity oscillations can be observed in all of the measurements, which is characteristic of interference effects. This is due to reflections from the polymer surface and the polymer-silica interface, which leads to two-beam interference. At incident angle $\theta_i = 0^o$, the transmission enhancement for the nanostructured interface is not obvious, as shown in Figure 4(a). However, the intensity oscillation is reduced. This can be attributed to the reduction of reflection at the polymer-silica interface by the nanostructures, thereby suppressing interference effects. The transmittance measurement for incident angle $\theta_i = 30^o$ shows an average of 5% transmission enhancement for the sample with the interfacial nanostructures, as shown in Fig. 4(b). It can also be observed that the intensity oscillation has also been reduced. These results indicate that the sample with nanostructured interface has higher light transmission and less intensity oscillation due to interference effects.

The interference contrast, or the ratio of the sinusoidal intensity amplitude to the average intensity, can be calculated to quantify the suppression of the thin-film interference effects. The contrast describes the degree of interference for the reflected orders, and approaches 0 as the interfacial reflection is suppressed [29]. The contrast values are determined by first fitting the broadband transmittance data using a second order polynomial to estimate the average intensity. The difference between the data and the average intensity can then be calculated to approximate the sinusoidal intensity amplitudes. The contrast of the experimental data can then be defined as the ratio of the amplitude to the average intensity. We focus on the 450 to 750 nm range, since the sinusoids are not well defined at the long wavelength limit. The calculated contrast values for the samples with and without interfacial nanostructures are plotted in Fig. 5. The theoretical contrast values predicted using RCWA are also plotted. For the nanostructured interface samples, the structure profile was estimated from the SEM images. The planar samples were modeled as a semi-infinite silica substrate with a thin homogeneous polymer layer, allowing for the calculation of the thin-film interference. The substrate thickness in both cases is assumed to be longer than the coherent length of the light source, therefore the reflection orders at the back side of the substrates do not interfere. The reflection efficiencies were modeled using Fresnel equations to account for the losses in the theoretical transmission. A third model with linear taper profile was also included, demonstrating that further interference mitigation is possible with improved nanostructure profile.

The experimentally measured contrast data for both planar and nanostructured interfaces fit well to the simulation models. These results indicate that the interference

contrast of the samples with interfacial nanostructure can be reduced roughly by a factor of two compared to those without. The suppression of interference effects can also be observed at both incident angles of 0º and 30º incident angles. The simulation result also shows that with improved nanostructure height and profile, the contrast can be reduced further by a factor of 10. These results indicate interfacial nanostructure is effective to suppress interference effect, which can eliminate iridescent appearance and wavelength/angle-dependent transmission.

Going beyond the suppression of thin-film interference, the interfacial nanostructures can also improve light transmission. To demonstrate this, we first characterize the transmission of the double-side patterned silica substrate using a 633 nm HeNe laser (Model 30995, Research Electro-Optics, Inc.). A rotation stage was used to rotate the sample to change the incident angles from 0° to 70° with 1° resolution. For incident angles larger than 70°, the illumination area exceeds the area of the nanostructure material, and therefore are not considered. A photodiode detector (Model 918D-UV-OD3, Newport Co.) was used to measure the transmitted light intensity. The transmission for both TE and TM polarizations were characterized. The measured transmission and theoretical model of single fused silica substrate with and without double-side patterned nanostructures are plotted in Fig. 6. It can be observed that the data agree well with the RCWA and Fresnel models for the samples with and without the nanostructures, respectively. For TE polarization, the transmission is enhanced by ~5% near normal incidence, and up to 20% at 60-70º incident angle range. For the maximum incident angle of 70º, the measured transmission for the sample with and without the nanostructures are 80% and 48%, respectively. However, the optical transmission of the nanostructured sample is lower for

TM polarization between 50-70º incident angle ranges. This can be attributed to the Brewster angle effect, where the transmission for the planar sample is 100%. The nanostructured sample, in comparison, has scattering losses due to fabrication defects. The measurement error range is within 1.5% based on multiple measurements.

The measured transmission and theoretical calculations for the thick 3-layer silica-polymer composite with and without the interfacial nanostructures are shown in Figure 7. The sample was fabricated by bonding three double-side patterned fused silica substrates with two epoxy layers, as illustrated in the inset diagram. Note in this case the theoretical models assume no interference occurs since the layers are thick, therefore the transmissions at the interfaces were simulated separately and multiple together to yield the total transmission. The experiment results show that under illumination TE polarized light, the transmission is enhanced by 7% at normal incidence, and up to 30% at 60-70º incident angle ranges. For the maximum incident angle of 70º, the measured transmission for the composite with and without the nanostructures are 72% and 46%, respectively. For TM-polarized light similar enhancement for the planar interface sample can be observed due to Brewster angle, while the transmission for the nanostructured interface sample reduces monotonically at increasing incident angles. The measurement error bar is within 1% based on multiple measurements. The simulation model also demonstrates that near-perfect transmission can be maintained at highly oblique incident angles for taller interfacial nanostructures with a more effective tapper profile for both polarizations.

It is important to note that the transmission enhancement for 3 layer is not significant due to the relatively similar index of fused silica and epoxy used. However, the improvement would be significant at higher number of layers. The theoretical transmission

for 5, 10, and 20 layers with planar and nanostructured interface are plotted in Figure 8, which illustrates significant enhancement. The nanostructure is modeled to have 750 nm height with a linear taper profile. The transmission of the sample with planar interface degrades significantly. However, the transmission can be maintained at near unity even at high incident angle for the corresponding composite with interfacial nanostructures. These results demonstrate that the interfacial nanostructures are effective in suppressing the reflection at the multiple polymer-silica interfaces to enhance overall transmission. Enhancement in more number of layers would yield higher transmission enhancement, and is the subject of on-going research.

The broadband transmittance of the thick 3-layer silica-polymer composite with and without the nanostructures at the interfaces were also characterized at normal incidence, as shown in Fig. 9. Here it can be observed that the transmission across broad wavelength band can be enhanced. The measurement data illustrates that up to 7% enhancement can be observed at 450 nm to 800 nm wavelength, with a peak transmission of 97% compared with 90% without the nanostructures. The enhancement is reduced at wavelength below 450 nm, and the transmission of the two samples are similar. This can be attributed to the relatively large structure period of 250 nm, which means diffracted orders in the UV can exist in the higher index polymer. The UV-curable epoxy also absorbs in the UV, therefore reducing transmission for both samples. Note the thickness of the fused silica and epoxy layers are approximately 0.5 mm and 0.1 mm, respectively, but some variations in the epoxy can occur during the bonding process. Due to the relative thick layers, thin-film interference effects are not observed. However, interference effects can still be present if the multilayer composites are under illumination from a light source with higher coherence.

These results and the derived models indicate that by using interfacial nanostructures, the reflection between two materials can be successfully suppressed. This effect in turn suppresses interference in multilayer composites, allowing for wavelength and angle-independent optical behavior. For better interfacial antireflection effects than those demonstrated, taller structures [12] with an optimal taper profile can be used [33,34]. While the experimental data follow the trends predicted by the RCWA and Fresnel equation, errors can be observed. This can be attributed to the defects of the nanostructures. The proposed fabrication methods based on IL and RIE can be scalable, and full wafer patterning is possible. However, the defect areas from multiple samples can compound after bonding, resulting in scattering losses. We believe this may lead to the transmission enhancement being slightly lower than theoretical models. However, the existence of these mismatches does not prevent demonstration of the transmission enhancement of multilayer composites with interfacial nanostructure, which is the main focus of this study.

For future work, different mask materials will be used to fabricate taller interfacial nanostructures with height over 700 nm for better AR effects at longer wavelength and more oblique incident angles. The interfacial nanostructures with shorter period less than 200 nm can also reduce the diffraction and therefore improve the optical transmission in UV region. The profile of the structure will also be fine-tuned to obtain a wider range of tapered width. The yield will also be improved to reduce scattering losses and further enhance transmission. In addition, composite samples with more layers will be tested to demonstrate scalability and achieve higher transmission enhancement. The nanostructured interface can also have novel mechanical and thermal properties, which is the subject of on-going research.

CONCLUSION

In this study, we demonstrate that interfacial nanostructure in multilayer composite stacks can reduce interfacial reflections, suppress interference effects, and enhance light transmission. This is supported by experimental characterization and theoretical modeling of light transmission in thin and thick multilayer films consisting of nanostructured interface between neighboring silica and polymer layers. The experimental data show that the interference contrast observed in the transmittance of thin films can be suppressed by a factor of two, and thick 3-layer silica-polymer composites can exhibit transmission enhancement up to 30% at 60-70º incident angle range. The enhancement is also broadband, and the fabricated interfacial nanostructures show higher transmission from 450-800 nm wavelength. This work demonstrated that interfacial nanostructures can reduce reflection losses in multilayers composites, increasing transmission and suppressing iridescence. This can mitigate wavelength and angle-dependence behaviors and enhance broadband transmission in multilayer photonic element and devices.

ACKNOWLEDGEMENT

This work was performed in part at the NCSU Nanofabrication Facility (NNF) and the Analytical Instrumentation Facility (AIF), members of the North Carolina Research Triangle Nanotechnology Network (RTNN), which is supported by the National Science Foundation as part of the National Nanotechnology Coordinated Infrastructure (NNCI). This work was supported by the Army Research Office (ARO) under grant W911NF-17-1-0591 and partially supported by National Science Foundation (NSF) grant CMMI#1552424.

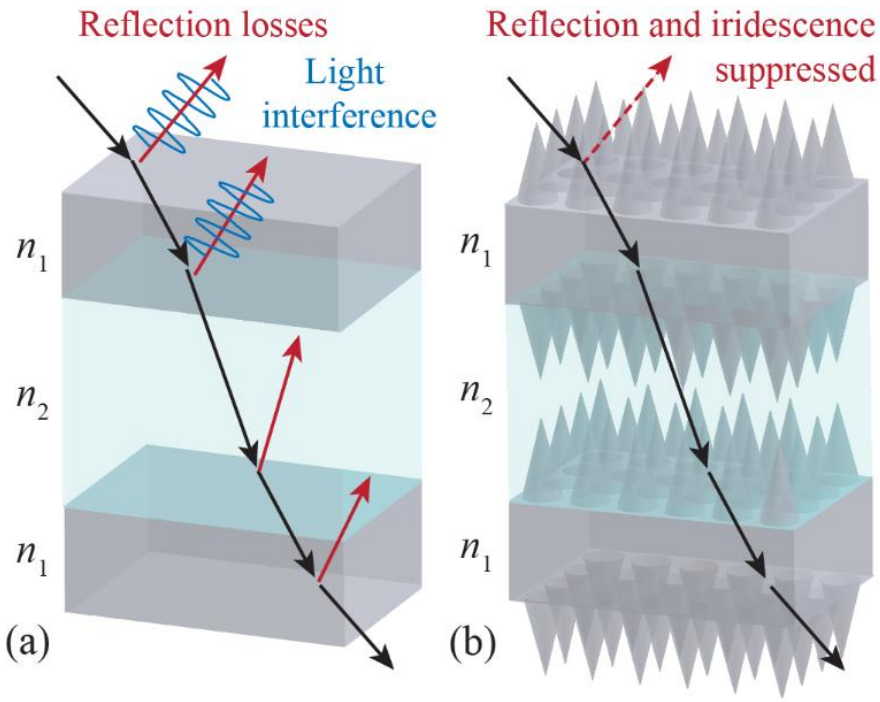

Figure 1. Schematic of (a) Fresnel losses and light interference in multilayer films with alternating materials with planar interfaces. (b) The reflection and iridescence can be suppressed using interfacial nanostructures.

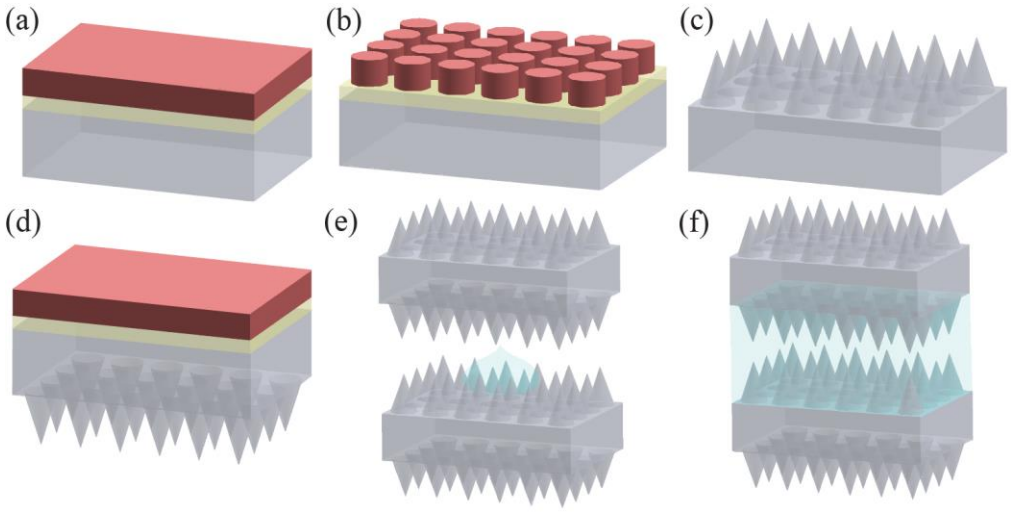

Figure 2. Schematic of fabrication process. (a) Spin coat ARC and photoresist. (b) Pattern 2D pillar array in photoresist using IL. (c) Etch pattern into fused silica substrate using RIE. (d) Spin coat ARC and photoresist on back surface. (e) Bound double-side patterned fused silica samples using NOA. (f) Fused silica/polymer composite with interfacial nanostructures.

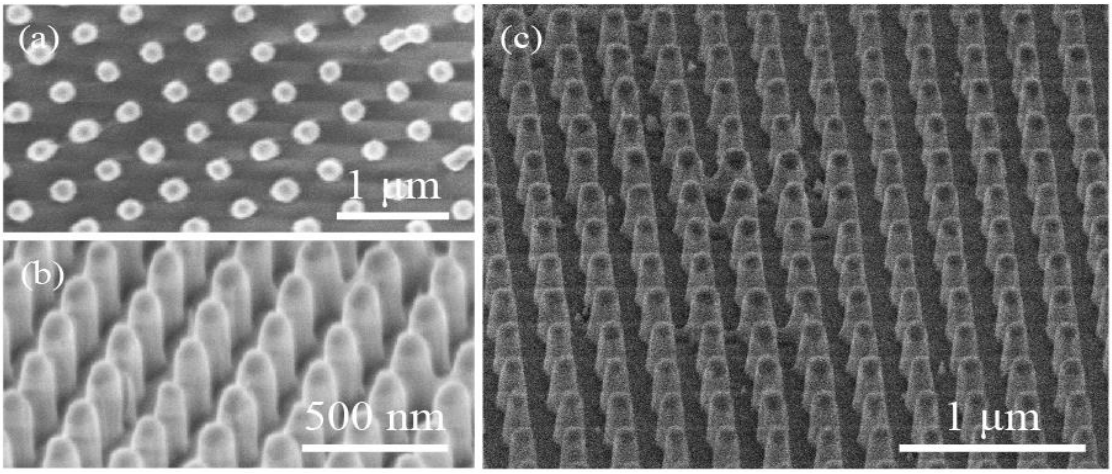

Figure 3. SEM images of fabricated samples. (a) Top-view image of 2D pillar array in photoresist, (b)-(c) side-view images of 2D taper nanostructures etched into fused silica substrate.

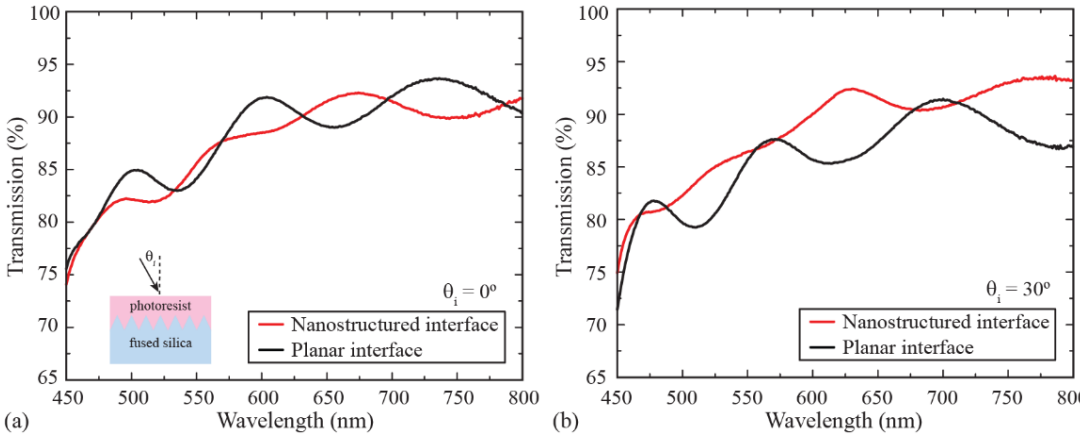

Figure 4. Broadband measurement data for thin polymer film on fused silica substrates with nanostructured and planar interfaces at incident angles (a) $\theta_i = 0^o$ and (b) $\theta_i = 30^o$. The film is a layer of photoresist with 750 nm thickness.

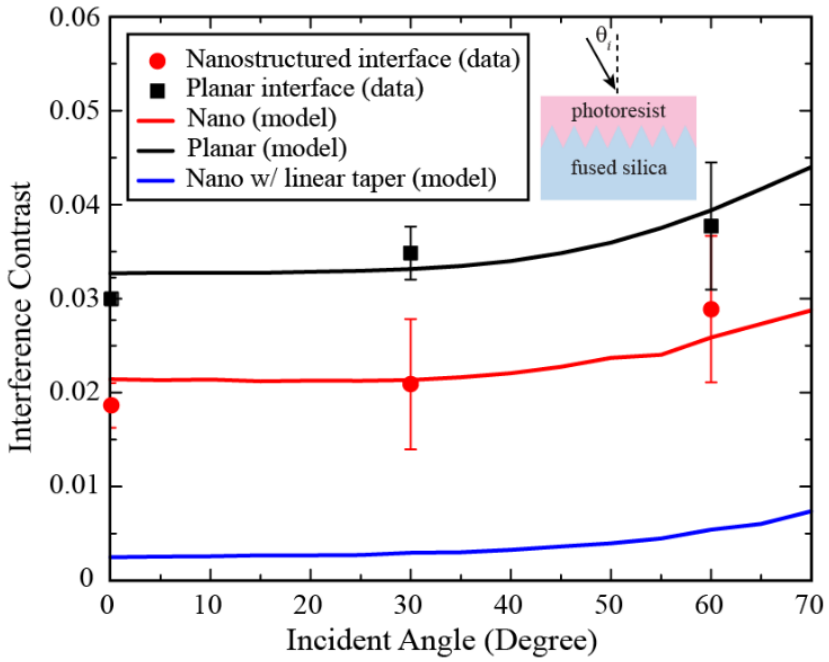

Figure 5. Measured interference contrast for thin polymer film on fused silica substrates with nanostructured and planar interfaces. The simulations models for fabricated nanostructure, planar, and ideal linear taper are also shown.

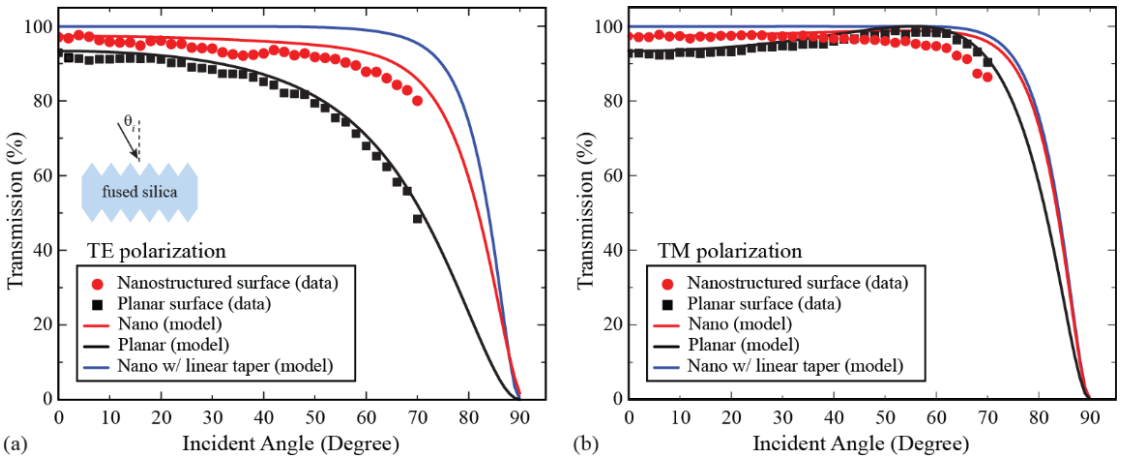

Figure 6. Transmission measurement and simulation under different incident angles for fused silica substrate with and without double-side nanostructures for (a) TE and (b) TM polarization.

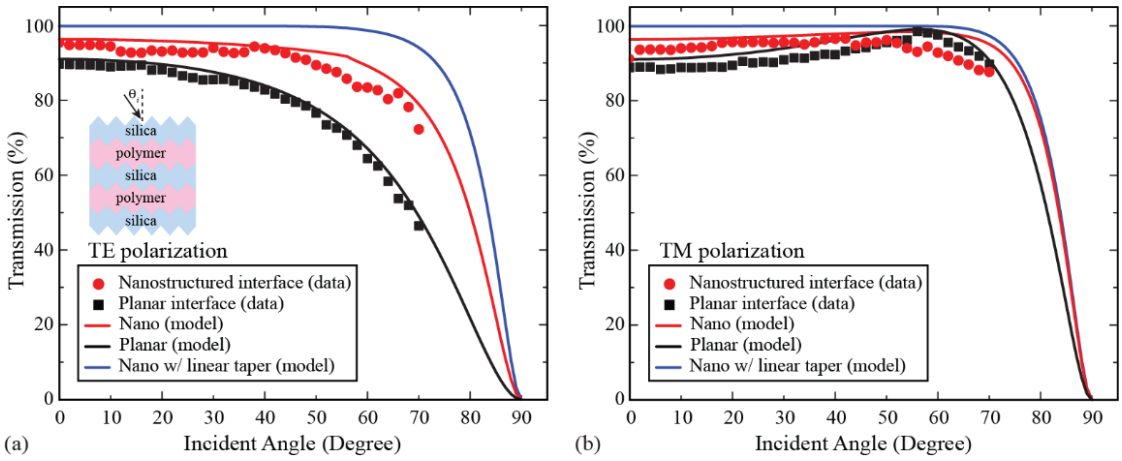

Figure 7. Transmission measurement and simulation under different incident angle for a thick 3-layer silica-polymer multilayer composite with and without interfacial nanostructures for (a) TE and (b) TM polarization.

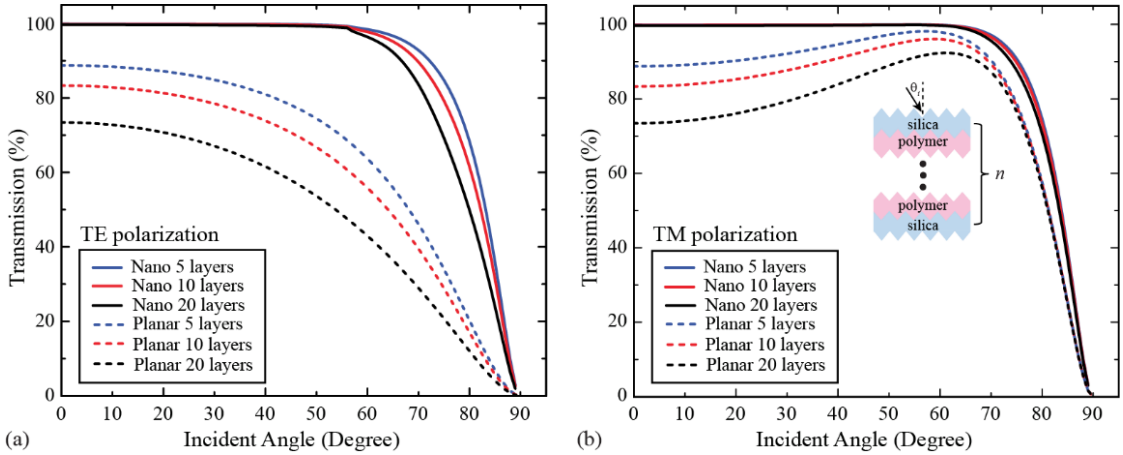

Figure 8. Transmission simulation under different incident angle for 5, 10, and 20 layer thick silica-polymer composite with and without interfacial nanostructures for (a) TE and (b) TM polarization.

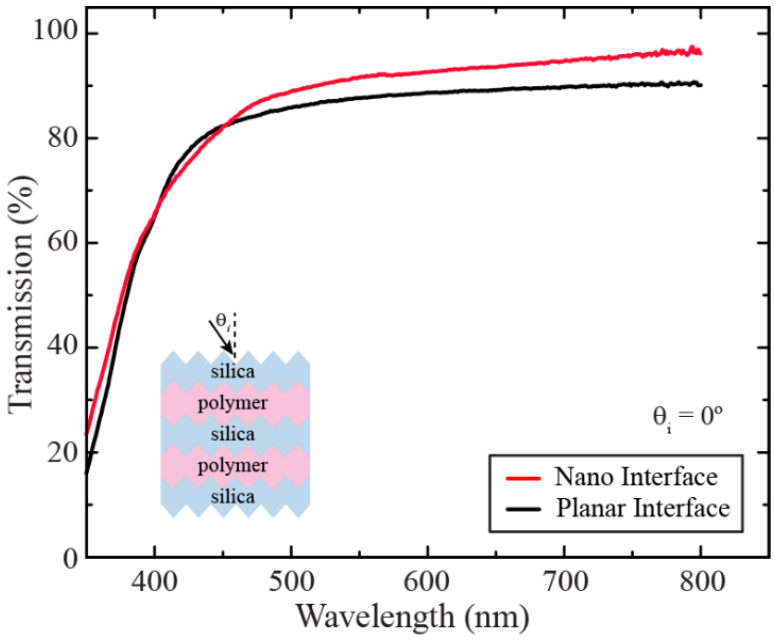

Figure 9. Broadband transmittance measurements of a thick 3-layer silica-polymer multilayer composite with and without interfacial nanostructure at 0º incident angle.

REFERENCES

[1] P.B. Clapham, M.C. Hutley, Nature **1973** *244* 281–282.
[2] S.J. Wilson, M.C. Hutley, Opt. Acta **1982** *29* 993–1009.
[3] D.H. Raguin, G.M. Morris, Appl. Opt. **1993** *32* 1154–1167.
[4] P. Lalanne, G.M. Morris, Nanotechnology **1997** *8* 53–56.
[5] Y. Kanamori, M. Sasaki, K. Hane, Opt. Lett. **1999** *24* 1422–1424.
[6] P. Vukusic, J.R. Sambles, Nature **2003** *424* 852–855.
[7] D.G. Stavenga, S. Foletti, G. Palasantzas, K. Arikawa, Proc. R. Soc. B Biol. Sci. **2006** *273* 661–667.
[8] A.R. Parker, H.E. Townley, Nat. Nanotechnol. **2007** *2* 347–353.
[9] S.A. Boden, D.M. Bagnall, Appl. Phys. Lett. **2008** *93* 133108.
[10] J.-Q. Xi, M.F. Schubert, J.K. Kim, E.F. Schubert, M. Chen, S.-Y. Lin, W. Liu, J.A. Smart, Nat. Photonics **2007** *1* 176–179.
[11] Y.M. Song, S.J. Jang, J.S. Yu, Y.T. Lee, Small **2010** *6* 984–987.
[12] K.-C. Park, H.J. Choi, C.-H. Chang, R.E. Cohen, G.H. McKinley, G. Barbastathis, ACS Nano **2012** *6* 3789–3799.
[13] S. Chattopadhyay, Y.F. Huang, Y.J. Jen, A. Ganguly, K.H. Chen, L.C. Chen, Mater. Sci. Eng. R Rep. **2010** *69* 1–35.
[14] W. H. Southwell, J. Opt. Soc. Am. A **1991** *8* 549-553.
[15] D. Poitras, J.A. Dobrowolski, Appl. Opt. **2004** *43* 1286–1295.
[16] A. Bagal, X.A. Zhang, R. Shahrin, E.C. Dandley, J. Zhao, F.R. Poblete, C.J. Oldham, Y. Zhu, G.N. Parsons, C. Bobko, C.-H. Chang, Sci. Rep. **2017** *7* 9145.
[17] C.-H. Sun, P. Jiang, B. Jiang, Appl. Phys. Lett. **2008** *92* 061112.
[18] H. Park, D. Shin, G. Kang, S. Baek, K. Kim, W.J. Padilla, Adv. Mater. **2011** *23* 5796–5800.
[19] Y.-F. Huang, S. Chattopadhyay, Y.-J. Jen, C.-Y. Peng, T.-A. Liu, Y.-K. Hsu, C.-L. Pan, H.-C. Lo, C.-H. Hsu, Y.-H. Chang, C.-S. Lee, K.-H. Chen, L.-C. Chen, Nat. Nanotechnol. **2007** *2* 770–774.
[20] M.-L. Kuo, D.J. Poxson, Y.S. Kim, F.W. Mont, J.K. Kim, E.F. Schubert, S.-Y. Lin, Opt. Lett. **2008** *33* 2527–2529.
[21] X.A. Zhang, Y.-A. Chen, A. Bagal, C.-H. Chang, Opt. Lett. **2017** *42* 4123–4126.
[22] Q. Xu, V.R. Almeida, R.R. Panepucci, M. Lipson, Opt. Lett. **2004** *29* 1626–1628.
[23] J.K. Kim, T. Gessmann, E.F. Schubert, J.-Q. Xi, H. Luo, J. Cho, C. Sone, Y. Park, Appl. Phys. Lett. **2006** *88* 013501.
[24] J. Zhu, C.-M. Hsu, Z. Yu, S. Fan, Y. Cui, Nano Lett. **2009** *10* 1979–1984.
[25] K.X. Wang, Z. Yu, V. Liu, Y. Cui, S. Fan, Nano Lett. **2012** *12* 1616–1619.
[26] M.G. Deceglie, V.E. Ferry, A.P. Alivisatos, H.A. Atwater, Nano Lett. **2012** *12* 2894–2900.
[27] J. Tippens, A. Bagal, X.A. Zhang, C.-H. Chang, Opt. Express **2017** *25* A840–A850.
[28] P. Pignalosa, B. Liu, H. Chen, H. Smith, Y. Yi, Opt. Lett. **2012** *37* 2808–2810.
[29] Q. Yang, X.A. Zhang, A. Bagal, W. Guo, C.-H. Chang, Nanotechnology **2013** *24* 235202.
[30] M.G. Moharam, E.B. Grann, D.A. Pommet, T.K. Gaylord, J. Opt. Soc. Am. A **1995** *12* 1068–1076.
[31] M.G. Moharam, D.A. Pommet, E.B. Grann, T.K. Gaylord, J. Opt. Soc. Am. A **1995** *12* 1077–1086.

[32] H.I. Smith, Phys. E Low-Dimens. Syst. Nanostructures **2001** *11* 104–109.
[33] E.B. Grann, M.G. Moharam, D.A. Pommet, J. Opt. Soc. Am. A **1995** *12* 333–339.
[34] Y. Zhang, C. Li, M. Loncar, Opt. Lett. **2013** *38* 646–648.